ARTICLE

BIOTECHNOLOGY and BIOENGINEERING

Understanding Tissue Specific Compositions of Bioenergy Feedstocks Through Hyperspectral Raman Imaging

Lan Sun,[1,2] Blake A. Simmons,[1,2] Seema Singh[1,2]

[1]Physical Biosciences Division, Joint BioEnergy Institute, Lawrence Berkeley National Laboratory, 5885 Hollis Street, Emeryville 94608, California; telephone: 925-337-1453; fax: 925-294-3020; e-mail: seesing@sandia.gov

[2]Biomass Science and Conversion Technology Department, Sandia National Laboratories, P.O. Box 969, Livermore 94551, California

Received 23 May 2010; revision received 18 August 2010; accepted 23 August 2010

Published online 7 September 2010 in Wiley Online Library (wileyonlinelibrary.com). DOI 10.1002/bit.22931

ABSTRACT: Hyperspectral Raman imaging was used to study the tissue/cell type specific distribution of lignin and cellulose polymers within the plant cell walls. Distinct differences in cell wall compositions were identified between two potential bioenergy feedstocks: corn stover and *Eucalyptus globulus*. Characteristic bands of 627, 1,175, 1,206, and 1,428 cm^{-1} were only observed for corn stover and 1,381 cm^{-1} was only present in *E. globulus*. One-dimensional and two-dimensional chemical maps of lignin and cellulose were generated for the stem of corn stover, ranging from the epidermis to the pith area and revealed that lignin and cellulose abundance varies significantly among different cell types in the following order: sclerenchyma cells and tracheids (~5 times) > epidermal cells (~3 times) > bundle sheath cells > parenchyma cells. The Raman mapping methods developed on corn stover were also validated on *E. globulus* and clearly highlighted their difference in lignin composition.

Biotechnol. Bioeng. 2011;108: 286–295.

KEYWORDS: hyperspectral raman imaging; cell walls; lignin; cellulose; tissue and cell type

Introduction

One of the world's greatest energy challenges today is to reduce the dependence on fossil fuels. This challenge can be met by transitioning domestic, industrial, and transportation energy needs to renewable resources. Biofuels may help meet the requirements of sustainable development in the transportation sector due to their potential reduction of net emissions of greenhouse gases. To avoid competition with the food/feed supply, second-generation biofuels produced from lignocellulosic biomass have become the focus of significant R&D efforts worldwide (Gallezot, 2008; Tilman et al., 2006), because lignocellulose is a cheap, abundant, and underutilized source of sugars that can be used for biofuel production (Gomez et al., 2008). One of the major technical challenges for efficient biofuel production is to liberate the sugars from the complex cell wall matrix, which is composed of a cellulose microfibril framework tethered together by a coating of hemicellulosic polysaccharides and sealed in a waterproof and chemically durable polymeric matrix of lignin (Gomez et al., 2008; Somerville et al., 2004) and has evolved for strength and extreme recalcitrance to biochemical attack by living organisms (Himmel et al., 2007). Understanding and overcoming this recalcitrance in a cost-effective fashion is key to the realization of an advanced biofuel industry.

There are two major approaches that are being pursued to overcome this saccharification barrier. One approach is to modify the lignocellulosic biomass genetically to obtain enhanced characteristics amenable to efficient sugar conversion (Himmel et al., 2007; Simmons et al., 2008; Vanholme et al., 2008; Weng et al., 2008). The other approach is to develop optimal pretreatment processes (Dadi et al., 2006; Li et al., 2010; Teymouri et al., 2005; Wyman et al., 2005) and improve, discover and/or engineer lignocellulolytic enzymes for more efficient cell wall deconstruction (Percival Zhang et al., 2006; Spadiut et al., 2009). Previous studies have shown that the composition and structure of the cell wall varies within specific tissue/cell types in relation to growth and development (Freshour et al., 2003; Knox et al., 1990), and

Correspondence to: Seema Singh

Contract grant sponsor: Department of Energy, Office of Science, Office of Biological and Environmental Research DE-AC02-05CH11231

Contract grant sponsor: Lawrence Berkeley National Laboratory and the US Department of Energy

Additional Supporting Information may be found in the online version of this article.

that the plant cell wall components are not uniformly distributed within the cell walls (Williams et al., 1996). Therefore, to realize the rational design or re-engineering of plant cell walls via manipulation of biosynthetic pathways, one must first understand how these pathways affect the development and viability, and how the composition of the cell wall affects its deconstruction during pretreatment. To achieve this, detailed spatial and temporal mapping of pristine cell wall components within different tissue/cell types throughout development and during pretreatment is necessary.

Traditionally, plant cell wall compositions have been analyzed using numerous methodologies, such as chromatography (Fagard et al., 2000), mass spectrometry (Harvey, 2008), and nuclear magnetic resonance spectroscopy (Kim et al., 2008). Most of these methods are destructive and involve disruption of the plant tissue, separation of the cell wall from the rest of the cell components, or extensive chemical treatment of the plant cell walls. Various microscopic techniques can also be employed to acquire information about the plant cell wall, such as bright/dark field microscopy (D'Haeze et al., 2007), polarized light microscopy (Baskin et al., 2004), transmission electron microscopy (Fromm et al., 2003), scanning electron microscopy (Persson et al., 2007b), etc. However, to localize molecules of interest, histochemical and cytochemical staining and other traditional labeling methods have to be applied (Cavalier et al., 2008; Grünwald et al., 2002; Persson et al., 2007a). Although auto-fluorescence of lignin can be utilized to visualize distribution of lignin in the cell wall by fluorescence microscopy (Cavalier et al., 2008; De Micco and Aronne, 2007; Singh et al., 2009), chemical information of cellulose cannot be obtained without additional techniques and quantitative analysis is difficult. Therefore, a non-destructive and label-free method that is capable of providing tissue/cell type specific compositional and structural information would be extremely valuable for the plant cell wall research.

Vibrational microspectroscopic analysis, such as Raman and infrared imaging, offers chemical selectivity and is a very useful approach to meet the above criteria for plant cell wall research. Inelastic Raman scattering depends on changes in the polarizability of vibrating functional groups, while infrared absorption depends on changes of dipole moments (Smith and Dent, 2005). Infrared imaging has been applied to studies of plant growth and development as well as enzymatic treatment (Dokken et al., 2005; Gierlinger et al., 2008a). However, this technique is limited by low sensitivity due to non-background-free detection, low spatial resolution associated with the long infrared wavelengths, and water absorption of the infrared light (Evans and Xie, 2008). None of these limitations exist in Raman imaging, and both lignin and cellulose are Raman active and can be mapped simultaneously. Although auto-fluorescence from lignin may sometimes interfere with Raman measurement, the use of a near infrared or UV wavelength or a fluorescence quencher and effective baseline correction afterwards can alleviate this problem generally. Many examples of Raman spectroscopy (Agarwal and Ralph, 1997; Czaja et al., 2006; Tirumalai et al., 1996) and microspectroscopy (Agarwal, 2006; Gierlinger et al., 2008b; Gierlinger and Schwanninger, 2006; Schmidt et al., 2009) have been reported in the scientific literature that highlights Raman technique for plant cell wall research. In the present study, we demonstrate for the first time how hyperspectral Raman imaging can be employed to provide tissue/cell type specific information on the composition and ultrastructure of the plant cell wall. Two potential bioenergy feedstocks, corn stover and *Eucalyptus globulus*, were used. One-dimensional (1D) profiles of lignin and cellulose were generated for the stem of corn stover ranging from the epidermis to the pith, encompassing all different tissue/cell types, and for the xylem tissue of *E. globulus*, including tracheids and vessel elements. Two-dimensional (2D) Raman mapping was then conducted for both feedstocks to reveal detailed tissue/cell type specific compositional and ultrastructural information and to compare the compositions of these two systems.

Materials and Methods

Sample Preparation

Corn stover samples were generously supplied by the USDA ARS Albany Plant Gene Expression Center (Laboratory of Dr. Sara Hake). *E. globulus* chips were kindly provided by ArborGen (Summerville, SC) as a gift. The 100 μm-thick sections of corn stover stem and 50-μm-thick sections of *E. globulus* stem were sliced from samples as received on a vibratome (Leica VT1000S, Bannockburn, IL) and imaged without any further sample preparation. All the images shown in this work were from the same sections of corn stover and *E. globulus* stems.

Raman Analysis

Raman spectra and Raman mapping were acquired with a LabRam HR 800 confocal Raman system (Horiba Jobin Yvon, Edison, NJ). This integrated Raman system is equipped with a 785 nm diode laser, an Olympus IX71 inverted confocal microscope, and a high-precision nanopositioning piezo stage (P-562 PIMars) with a sub-nanometer high-resolution Raman imaging capability. A 40× (NA 0.75) objective and a high numerical aperture 100× (oil NA 1.40) objective were used. The chosen spectroscopic resolution was $\sim 4\,cm^{-1}$. For spectroscopic analysis, the 40× objective was used. Extended integration times (100 s for the corn section and 150 s for the *E. globulus* section) were implemented to acquire spectra with sufficient detail without saturating the detector, and an accumulation number of 3 was applied to increase the signal-to-noise (S/N) ratio. For Raman imaging, the raster mapping technique was utilized with an exclusive SWIFT mode (the stage triggers the detector at specific positions and acquisition is done "on the fly") to significantly increase mapping speed. After parameter optimization, an integration

time of 1 s and a mapping step of 1 μm for a length of 80 μm (corn stover) or 60 μm (*E. globulus*) was chosen for 1D profiling using the 40× objective. An integration time of 1 s and a mapping step of 0.5 μm for a 10 by 10 μm region was chosen for the tissue/cell type specific 2D Raman mapping using the 100× objective.

The LabSpec5 software was used for establishing measurement and data processing. The spectra were baseline corrected and smoothed using the Savitsky–Golay algorithm for spectroscopic analysis revealing finer structures of biomass. The chemical images were achieved by integrating over defined wavenumbers of a series of spectra. The raw data were baseline corrected and de-spiked. Smoothing filtration was performed using the Savitsky–Golay algorithm at a moderate level and Fourier smoothing coupled with cosine apodization function. The image contrast was further improved in OriginPro 8 by applying a histogram contrast routine.

Results and Discussion

Raman Characterization of Lignocellulosic Feedstocks

Raman microspectroscopy can be used to provide a spatial distribution of intact plant cell wall components in their native form. Cellulose and lignin were chosen for Raman spectral analysis because cellulose is the major source of sugar for biofuel production and lignin, interwoven with cellulose and hemicellulose, is one of the primary sources of recalcitrance in biomass. In order to understand the Raman spectra from corn stover and *E. globulus*, standard spectra from model cellulose and lignin compounds were first acquired. The standard Raman spectrum (Fig. S1, Supporting Information) of cellulose was obtained from Avicel (high purity microcrystalline cellulose). The characteristic bands are summarized in Table I and are in agreement with data reported in the literature (Agarwal and Ralph, 1997). Lignin is a complex and heterogeneous biopolymer lacking a defined primary structure and is composed primarily of *p*-hydroxyphenyl (H), guaiacyl (G), and syringyl (S) units. The S:G:H ratio of the plant tissue varies greatly among feedstocks and is believed to be one of the primary reasons for variations in biomass recalcitrance (Davison et al., 2006). Therefore, distinguishing these structures in lignin is very important to understand lignin:polysaccharide interaction in the cell wall and to track its deconstruction. Raman microspectroscopy can be used to identify these different structures without the need for extensive extraction and depolymerization, and to provide a spatial distribution of these structures in intact plant cell walls. We selected nine model compounds (Saariaho et al., 2003) that represent common H, G, and S structures to use as Raman standards. The repeating Raman bands from each group of the model compounds were assigned to the corresponding lignin structure. The detailed procedure is described in the Supporting Information (Figs. S2–S4 and Table SI), and the results are presented in Table I. The majority of the characteristic bands associated with the different lignin structures are in agreement with previous reports using ultraviolet resonance Raman spectroscopy (Saariaho et al., 2003). These different lignin structures also contribute together to other major lignin bands (Agarwal and Ralph, 1997). Table I is organized such that non-overlapping bands are listed in separate rows while overlapping bands are listed in the same rows for the convenience of spectral data interpretation, and only well separated band ranges can be exclusively assigned to specific structures, which are identified in Table I.

Table I. Characteristic Raman bands (cm^{-1}) of cellulose and different lignin structures.

Cellulose	*p*-Hydroxyphenyl	Guaiacyl	Syringyl
339			
	342–350		
			375–377
387			
444			
499			
523			
			530–535
			586–590
	643–648		
			783–817
	821–864		
899			
			909–917
973			
1,000			
	1,013–1,018[a]		
		1,030–1,038	
			1,038–1,043
1,098			
1,122			
1,154			1,144–1,154
	1,163–1,181	1,172–1,188	1,185–1,191
	1,213–1,219		
		1,266–1,275	
			1,331–1,334
1,342			
1,380		1,368–1,380	1,369–1,380
	1,381–1,387		
		1,451–1,454	1,453–1,461
1,462			
		1,509–1,517	1,507–1,517
2,892			

Exclusive bands of specific structures for characterization are in bold.
[a]Based on the visual observation of the results, not shown in literature.

To characterize corn stover and *E. globulus*, Raman spectra were obtained from tracheids of both feedstocks, one of the major cell types of xylem tissue. Based on the characteristic bands, we have identified chemical structures that are specific or common to these two feedstocks. Raman spectra of the corn stover stem and *E. globulus* stem are shown in Figure 1. The Raman bands from the different chemical structures are denoted by the letters in parentheses (H, *p*-hydroxyphenyl lignin structure; G, guaiacyl lignin structure; S, syringyl lignin structure; C, cellulose; L, lignin). Cellulose, *p*-hydroxyphenyl lignin structure and guaiacyl lignin structure can be determined unambiguously from Raman spectra. The syringyl lignin structure was identified

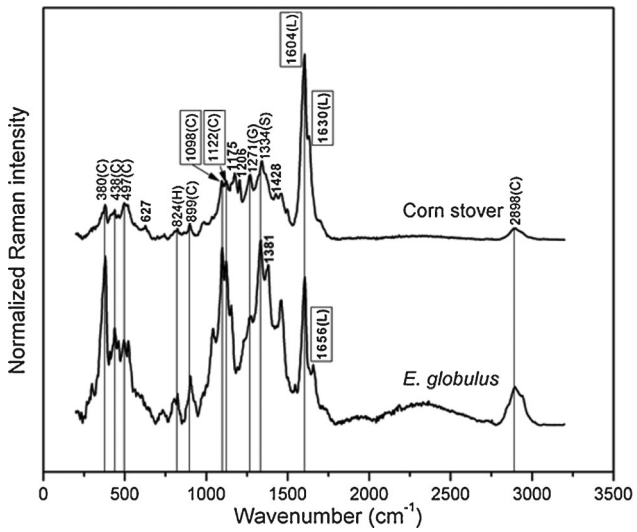

Figure 1. Raman characterization of the stem of corn stover and *E. globulus* with a spectral resolution of ~4 cm^{-1}. Characters in the parentheses indicate the assignments of the bands: (H), *p*-hydroxyphenyl lignin structure; (G), guaiacyl lignin structure; (S), syringyl lignin structure; (C), cellulose; (L), lignin. Bands marked by the rectangular boxes were used for imaging. Difference in the positions of the characteristic Raman bands between corn stover and eucalyptus are labeled in black.

in previous reports from both corn stover (Fenske et al., 1998) and *E. globulus* (Pinto et al., 2005) using other methods. Although the syringyl band around 1,334 cm^{-1} may be partially overlapped with the cellulose band at 1,342 cm^{-1}, especially for corn stover, this band can be resolved by standard band deconvolution methods.

There are two major lignin bands in the range of 1,600–1,660 cm^{-1} commonly used for lignin characterization in plants. The band around 1,600 cm^{-1} is attributed to a symmetric stretching of the aromatic ring. This is the most intense band for lignin since a diverse range of lignin structures contribute to it. The second band at ~1,620 cm^{-1} is typically attributed to the ring conjugated C=C stretching of coniferaldehyde. If the second band is observed at ~1,660 cm^{-1}, it is then typically assigned to either a ring conjugated C=C stretching of coniferyl alcohol or a C=O stretching of coniferaldehyde (Agarwal, 2006; Atalla and Agarwal, 1985; Gierlinger and Schwanninger, 2006). Although the spectra of corn stover and *E. globulus* share many characteristic bands, there are several major differences observed between these two plants: (1) a lignin band was observed at 1,630 cm^{-1} in corn stover and at 1,656 cm^{-1} in *E. globulus* section; (2) four Raman bands at 627, 1,175, 1,206, and 1,428 cm^{-1} were observed only in corn stover (the band of 1,428 cm^{-1} could be due to O–CH_3 deformation, CH_2 scissoring or guaiacyl ring vibration (Gierlinger and Schwanninger, 2006)); (3) a strong band at 1,381 cm^{-1} was observed only in *E. globulus*; and (4) intensity patterns of cellulose bands are different at 380, 1,098, and 1,122 cm^{-1}. These differences indicate that the cell wall composition and the interaction of different biopolymers in the cell wall are significantly different between corn stover and *E. globulus* stems.

Based on these results, 1D Raman profiles and 2D Raman chemical maps were acquired to study the distribution of lignin and cellulose inside the cell walls of different tissue/cell types. For the cross-section of corn stover, Raman band regions of 1,560–1,660 cm^{-1} and 1,070–1,140 cm^{-1} were used for investigating lignin and cellulose, respectively. For the cross-section of *E. globulus*, Raman band regions of 1,560–1,690 cm^{-1} and 1,070–1,140 cm^{-1} were used for investigating lignin and cellulose, respectively.

1D Profiling of Cell Walls

We employed Raman microspectroscopy to generate line profiles of the stem cross-sections to obtain an overview of lignin and cellulose distribution across various tissue/cell types. We developed the Raman mapping protocol using the corn stover stem, since it encompasses a variety of primary tissue types, including epidermis tissue of the dermal tissue system, sclerenchyma and parenchyma tissues of the ground tissue system, and xylem tissue of the vascular tissue system. Typical cell types studied here include ordinary epidermal cells of the epidermis tissue, parenchyma cells of the parenchyma tissue in the pith area, sclerenchyma cells of the sclerenchyma tissue ensheathing vascular bundles, tracheids of the xylem tissue, and bundle sheath cells of the bundle sheath tissue surrounding vascular bundles (Fig. 2a).

The line profile of the stem of corn stover is shown in Figure 3a. The top row of this figure displays the bright field video images of the same stem from the epidermis to the pith area, acquired using a 40× objective. Due to size limitations, the whole range in the *x*-direction is shown by four images. Movement of the stage was controlled to ensure that there is no shift in the *y*-direction, and that the four images are continuous along the *x*-direction (illumination is at the center of each image). The Raman 1D profiling was carried out along the line in the middle of the images with measurement positions at an interval of 1 μm. The Raman spectra collected were baseline corrected. The average signal-intensity (integrated Raman intensity divided by the selected wavenumber region) over the regions of 1,560–1,660 cm^{-1} and 1,070–1,140 cm^{-1} (with base value subtracted) was calculated to semi-quantitatively determine the amount of lignin and cellulose present. It should be noted that although the spectral region of 1,070–1,140 cm^{-1} for cellulose mapping has small contributions from hemicellulose, in order to obtain a stronger signal and the better S/N ratio and to reduce the experiment time we chose this region for integration as many other studies have (Agarwal, 2006; Gierlinger and Schwanninger, 2006). Agarwal (2006) has shown in his study that cellulose distribution profiled by this region is similar to that profiled by other cellulose band regions. Distribution of these components along the line is presented in Figure 3a. It was demonstrated in previous studies that the mechanical strength of the plant cell wall is

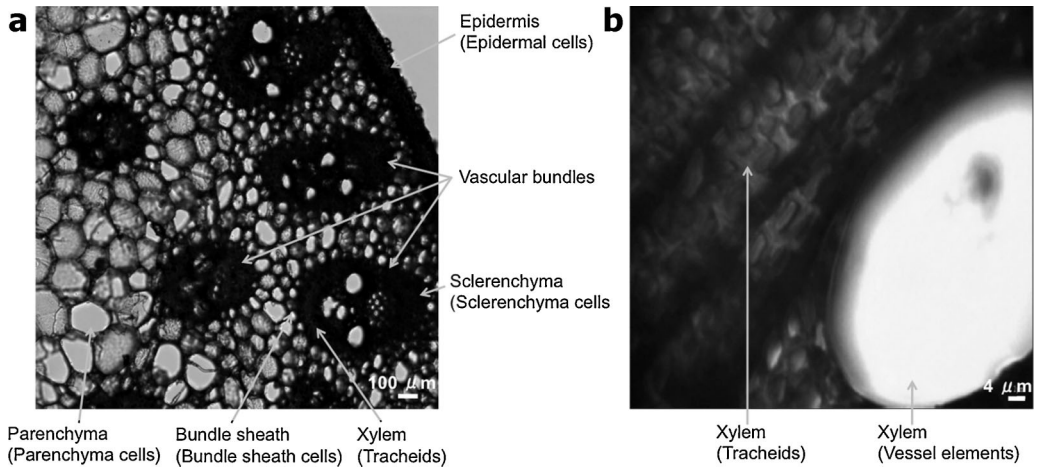

Figure 2. Video images of the tissues with the corresponding cell types (in the parentheses) selected for imaging in the stem cross-sections of (**a**) corn stover and (**b**) *E. globulus*.

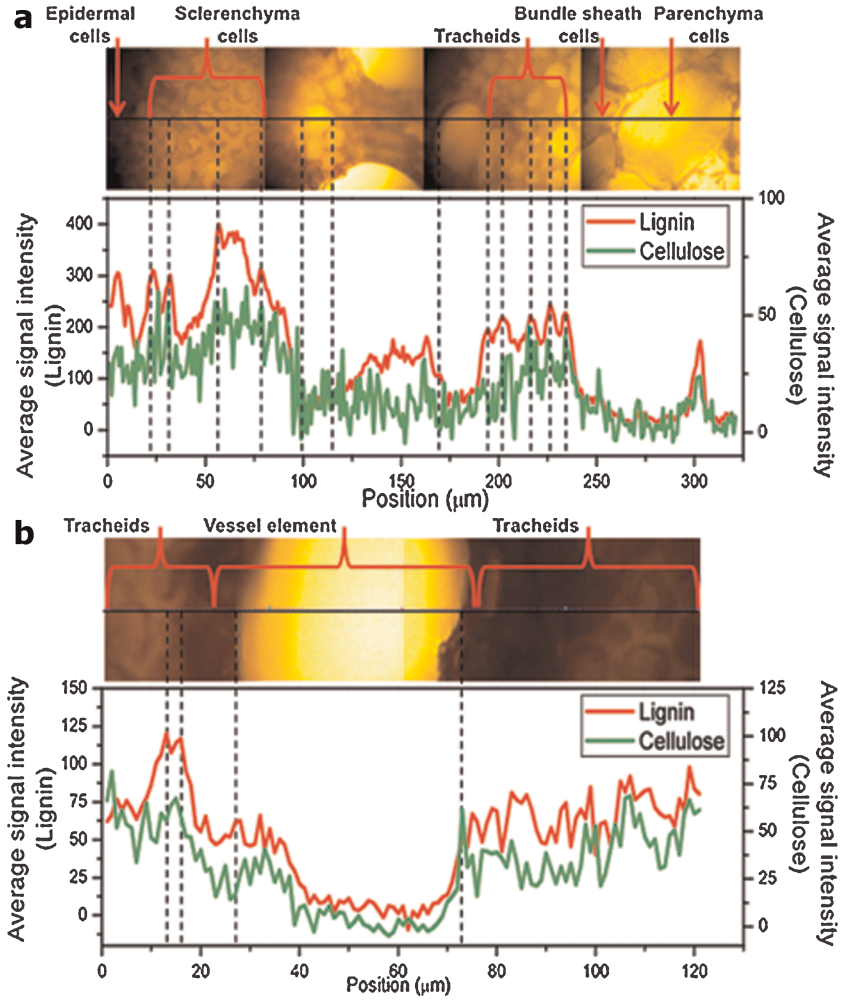

Figure 3. One-dimensional Raman profiles of lignin and cellulose across different cell tissue/cell types for (**a**) the corn stover stem and (**b**) the *E. globulus* stem.

related to its lignin and cellulose content (Jones et al., 2001; Turner and Somerville, 1997). For the line profile, the lignin content of cell walls is relatively high in the epidermis, which corroborates its role in providing mechanical support and stiffness to stems (Niklas and Paolillo, 1997). Sclerenchyma cells have higher lignin content, because the principal function of sclerenchyma is to support the stem structure (Evert, 2007). High lignin content was also observed in tracheids, one of the two fundamental types of tracheary elements in xylem for water transport due to their hydrophobic lignin coat. The bundle sheath cells and parenchyma cells are thin-walled cells and less lignified, and hence the lowest level of lignin was observed for these cells. 2D Raman mapping will provide a quantitative comparison of lignin distribution in different cell types. On the other hand, the distribution of cellulose signal follows the pattern of that of lignin, which could be explained by local tissue density and the strength and functions of cell walls for different tissue and cell types.

The most intense lignin peaks in Figure 3a correspond to cell corners (CCs), which are well known to have higher lignin content than other regions of the cell wall. The sharp peak around the 300 μm position that is located in a non-cell wall region could be due to the presence of a cell wall below the top surface of the cross-section, as that portion of the cross-section was not perfectly perpendicular to the longitudinal direction of the stem considering the shape and structure of the cell. This can also partially explain the data obtained in the sclerenchyma and xylem, where lignin signals were obtained in some non-cell wall regions. Signals from neighboring positions contribute to these non-specific lignin signals as well due to the large laser spot when using a 40× objective. A higher magnification objective with a higher numerical aperture, providing a smaller focal volume and a smaller laser spot size, could be used to resolve this issue and will be demonstrated in the 2D imaging discussion. Here a 40× objective was used to provide a

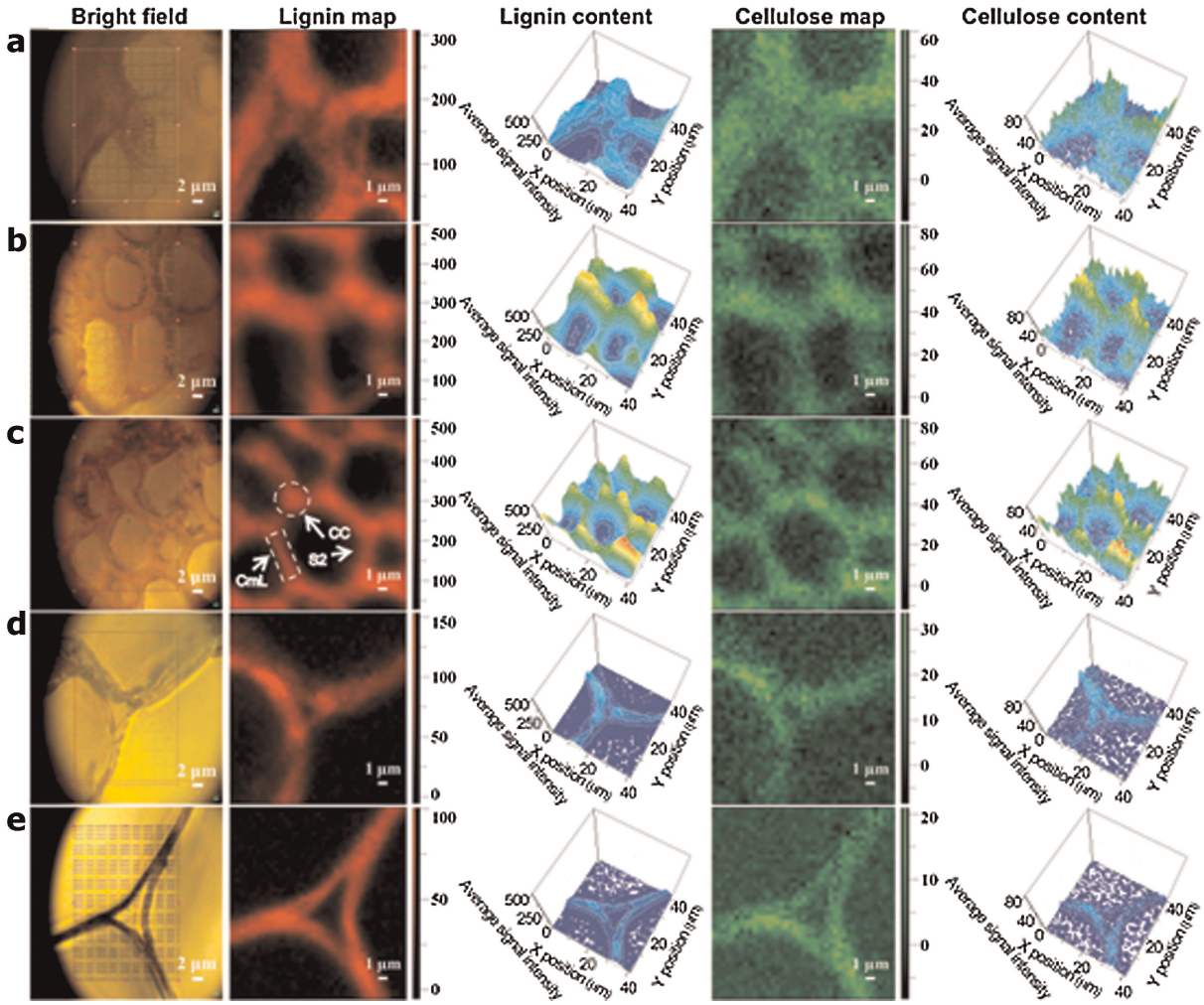

Figure 4. Two-dimensional Raman mapping of the stem of corn stover across different tissue/cell types. **a**: Epidermis (epidermal cells); (**b**) sclerenchyma (sclerenchyma cells); (**c**) xylem (tracheids); (**d**) bundle sheath (bundle sheath cells); (**e**) parenchyma (parenchyma cells).

wider view so that a complete profiling from the epidermis to the pith area is possible. This 1D profiling method was further validated on *E. globulus*. The xylem tissue (Fig. 2b) was selected for imaging and the obtained line profiles are shown in Figure 3b. The distribution of both lignin and cellulose contents is quite uniform, which is expected since only tracheids and a vessel element were examined and these cell types have similar functions. These results show that this method can simultaneously provide direct compositional information on multiple components across different tissue/cell types and can be applied to quite different feedstocks.

2D Compositional Mapping of Cell Walls

Although rough tissue/cell type specific information can be obtained by a complete line profile, detailed spatial insights into the ultrastructure and composition of the cell wall are critical to better understand the chemical, biological, and mechanical properties of plant cell walls. 2D hyperspectral Raman images with Raman spectra associated with each spatial position were generated for different tissue/cell types of corn stover and *E. globulus* stems (Fig. 2a and b).

The 2D compositional analysis for corn stover is shown in Figure 4. The columns of images from left to right exhibit bright field video images, lignin maps, three-dimensional (3D) color maps of lignin with average signal intensity (*z*-axis) and color codes (from blue to red: intensity from low to high) indicating the lignin content, cellulose maps and 3D color maps of cellulose showing cellulose content. The rows of images display the results for different tissues (cell types): (a) epidermis (epidermal cells), (b) sclerenchyma (sclerenchyma cells), (c) xylem (tracheids), (d) bundle sheath (bundle sheath cells), and (e) parenchyma (parenchyma cells). The plant cell wall has a multilayer structure consisting of the primary wall (P), secondary wall (S1, S2, and S3 with respect to the different orientation of cellulose microfibrils and chemical composition) and middle lamella (mL). The primary wall is thin and the mL is like an adhesive holding the neighboring cells together. The S2 secondary wall is the thickest and gives the rigid structure to the cell. Due to the diffraction-limited spatial resolution, only the S2 and CC regions could be sampled by themselves. The compound middle lamella (CmL) region investigated had contributions from the mL and adjacent primary walls and possibly some contribution from S1 depending on the thickness of the CmL region (Agarwal, 2006). All the 2D chemical maps were obtained using the 100× objective, which minimizes non-specific contributions from places outside of the focal plane. Thus, Raman signal from all the non-cell wall areas was close to zero. The lignin maps and the color-coded lignin content maps demonstrate that lignin content in CC areas is the highest for all tissue/cell types. The second highest level of lignin content is located in some spots of CmL and S2 areas. In other locations, the lignin content is significantly lower. The trends observed here agree well with data presented in the literature on woody samples (Agarwal, 2006; Gierlinger and Schwanninger, 2006). Interestingly, cellulose distribution follows the pattern of lignin distribution within different layers of the cell wall.

To obtain quantitative evaluation of lignin distribution in different tissue/cell types, three to six CC regions marked with 5 × 5 grids were selected from each lignin contour map (Figs. S5–S9, Supporting Information). CC regions were chosen to represent the lignin content of specific cell types, because the order of lignin content within other cell wall regions in different cell types is the same with CC regions based on the lignin maps presented in Figure 4, and it is easier to sample CC regions. The signal intensity of lignin was averaged over each marked CC region, which indicates the content level of lignin of the specific CC region. Then an average value was calculated for all the selected CC regions, which represents the content level of lignin of the specific cell type. Results presented in Figure 5a clearly show that the

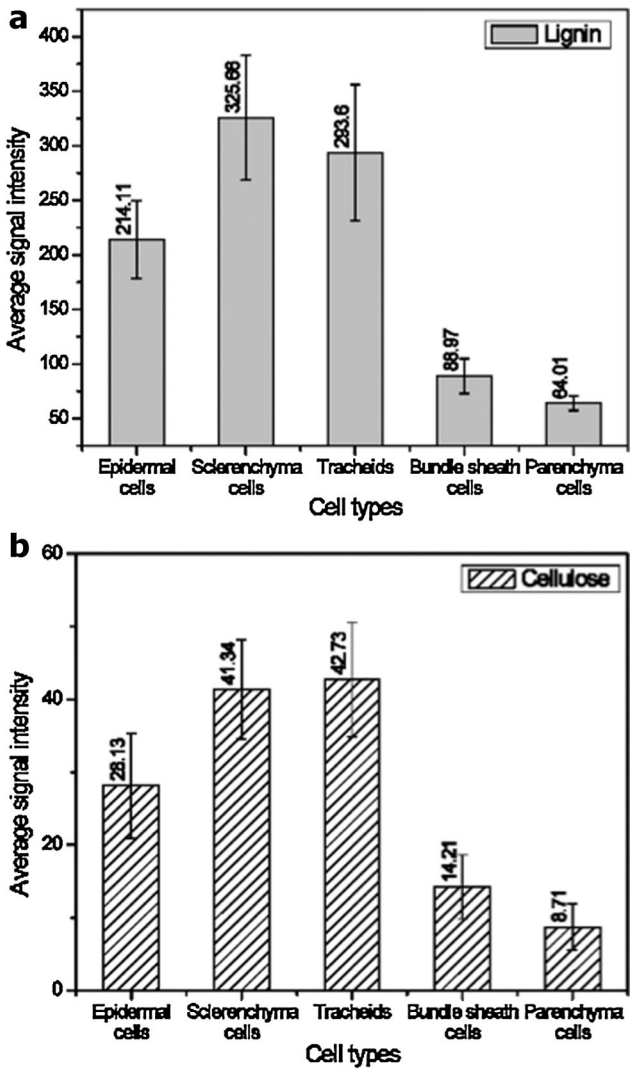

Figure 5. Comparison of content levels of cell wall components in different cell types of corn stover. **a**: Lignin; (**b**) cellulose.

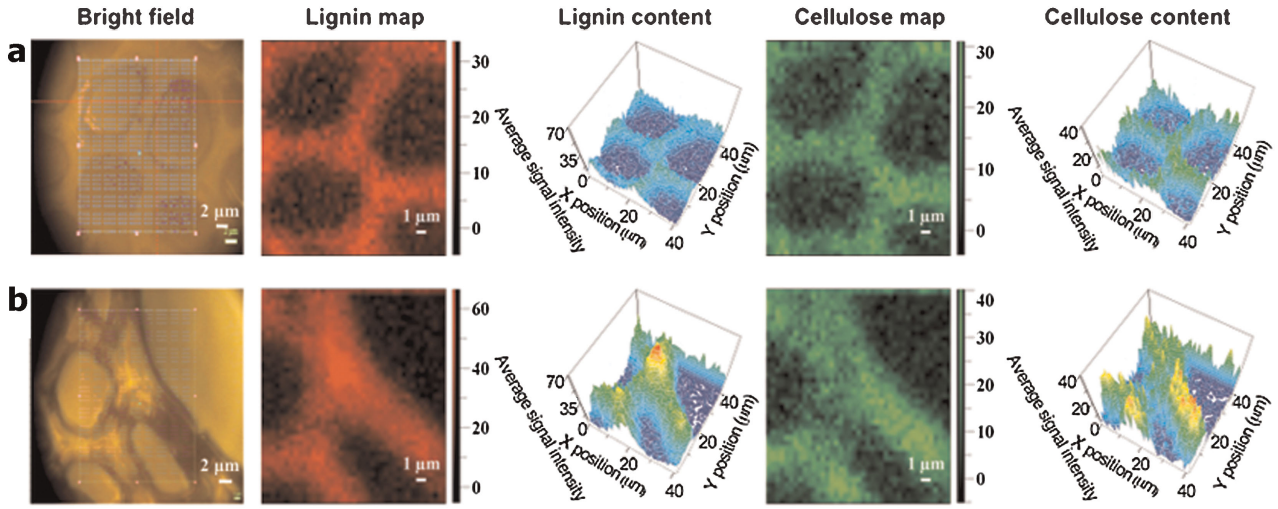

Figure 6. Two-dimensional Raman mapping of the xylem tissue of the *E. globulus* stem. **a**: Tracheids; (**b**) vessel element.

lignin content in different cell types is in the following order: sclerenchyma cells and tracheids > epidermal cells > bundle sheath cells > parenchyma cells, and the signal strength ratio is approximately 5:3.3:1.4:1. The same CC regions were used to calculate the signal levels for cellulose (Figs. S10–S14, Supporting Information), because cellulose distribution has a similar pattern to lignin distribution (Fig. 4). The same order of cellulose distribution in different cell types as that of lignin distribution was obtained with a similar signal strength ratio 5:3.2:1.6:1 (Fig. 5b). Although cellulose microfibril angle may also cause variability of the signal strength, it was expected that this variability is small compared to that caused by cellulose concentration. The distribution of lignin and cellulose across various tissue types can be explained by the functions of different tissues. For supporting, protection, and transportation functions, more rigid and enduring cell walls with higher lignin and cellulose content are necessary. The sclerenchyma is the principal mechanical element, the xylem is the principal water-conducting tissue, and the epidermis reduces water loss by transpiration, provides mechanical protection, and supports gaseous exchange through stomata. These tissues would therefore be expected to contain high to intermediate levels of lignin and cellulose. The bundle sheath and parenchyma do not have structural or transportation functions and therefore have lower lignin and cellulose levels (bundle sheath can carry out photosynthesis (Hibberd and Quick, 2002), and the parenchyma is the principal locus for many essential activities such as photosynthesis, assimilation, respiration, storage, etc. (Evert, 2007)).

The 2D Raman mapping was also applied to the xylem tissue of *E. globulus* as illustrated in Figure 6. The cell wall of the vessel element has a slightly higher lignin and cellulose content than that of the tracheid. For both cell types, CC regions have the highest lignin content followed by CmL and S2, while there is no obvious cellulose condensation at CC regions, which is consistent with the observations reported for the cell walls of poplar wood and black spruce wood (Agarwal, 2006; Gierlinger and Schwanninger, 2006). It is interesting to note that this is contrary to what was observed from corn stover (Fig. 4). These data indicate that perhaps the relation between lignin and cellulose distribution is species dependent.

The 2D Raman mapping can also be used to compare the compositional difference between different feedstocks. As

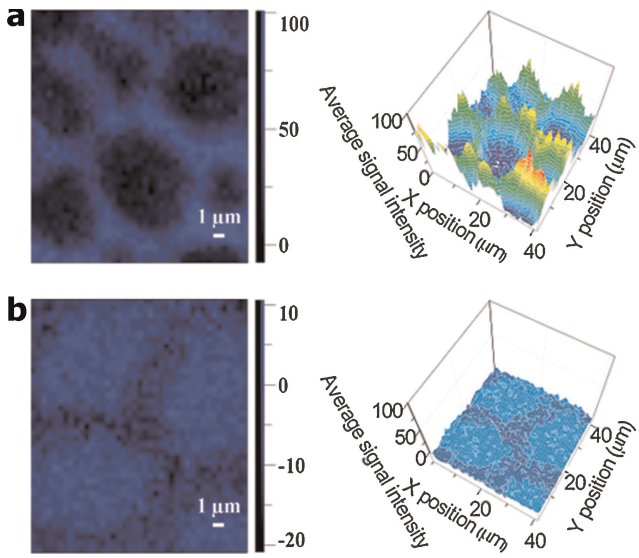

Figure 7. Comparison of the cell wall composition between corn stover and *E. globulus* stems using 2-D Raman imaging. **a**: Raman maps of tracheids of the corn stover stem based on integration over the region of 1,145–1,225 cm^{-1}; (**b**) Raman maps of tracheids of the *E. globulus* stem based on integration over the region of 1,145–1,225 cm^{-1}.

mentioned before, Raman bands at 1,175 cm^{-1} and 1,206 cm^{-1} were detected only in corn stover. By integrating over 1,145–1,225 cm^{-1}, a separate set of Raman images was generated for the tracheids of corn stover (Fig. 7a) and *E. globulus* (Fig. 7b). As expected, no signal was obtained for *E. globulus*, while the signal was clearly detected in the entire cell wall of corn stover. Although there are no conclusive assignments of the Raman bands at 1,175 cm^{-1} and 1,206 cm^{-1} yet, these bands could be due to the *p*-hydroxyphenyl lignin structure, based on the Raman characterization of model compounds (Table I). If so, there is a distinct difference in lignin polymerization involving *p*-hydroxyphenyl units between the cell wall of corn stover and that of *E. globulus*. Our hypothesis is supported by previous lignin compositional analyses showing that *E. globulus* contains a much lower ratio of *p*-hydroxyphenyl units than corn stover (Galletti et al., 1996; Pinto et al., 2005). One final note, rapid Raman mapping with an integration time of 1 s was used in this study. By increasing the integration time, more spatial chemical details can be revealed.

Conclusions

Hyperspectral Raman imaging was demonstrated for the first time as an effective tool to provide tissue/cell specific compositional and ultrastructural analysis of the plant cell wall in situ without using any labeling or staining agents. For the stem of corn stover, it was observed that lignin and cellulose content varies significantly among different cell types. The order from highest to lowest is: sclerenchyma cells and tracheids (approximately five times higher) > epidermal cells (approximately three times higher) > bundle sheath cells (slightly higher) > parenchyma cells. The ultrastructure of the cell wall was also examined in corn stover, with the highest lignin and cellulose content located in CC areas followed by the CmL and S2 areas. The vessel element has a higher lignin and cellulose content than the traicheids of the xylem tissue in the *E. globulus* stem. Unlike corn stover, in *E. globulus* cellulose is not concentrated at CC areas where there is the highest level of lignin content. Furthermore, significant compositional differences were observed between corn stover and *E. globulus*.

The method established in this research can be easily adopted to characterize genetically modified plants at the tissue level, and to understand the molecular mechanisms and optimize the procedures for chemical and enzymatic processing of cell wall components. The method is potentially applicable to various cell types. In conjunction with advanced multivariate data analysis tools, it is possible to obtain more detailed information on the composition and ultrastructure of the plant cell wall as well as interactions between cell wall components. Hyperspectral Raman imaging will contribute to fundamental understanding of the plant cell wall and generate valuable information for the bioenergy industry to achieve cost and time effective biofuel production.

The authors thank Dr. Umesh P. Agarwal and Dr. Notburga Gierlinger for their suggestions, Dr. Purbasha Sarkar for her help on sample preparation, and Dr. John Gladden, Dr. Huawen Wu, and Dr. Steven Singer for reviewing this manuscript. This work was part of the DOE Joint BioEnergy Institute (http://www.jbei.org) supported by the US. Department of Energy, Office of Science, Office of Biological and Environmental Research, through contract DE-AC02-05CH11231 between Lawrence Berkeley National Laboratory and the US Department of Energy.

References

Agarwal U. 2006. Raman imaging to investigate ultrastructure and composition of plant cell walls: Distribution of lignin and cellulose in black spruce wood (*Picea mariana*). Planta 224(5):1141–1153.

Agarwal UP, Ralph SA. 1997. FT-Raman spectroscopy of wood: Identifying contributions of lignin and carbohydrate polymers in the spectrum of black spruce (*Picea mariana*). Appl Spectrosc 51:1648–1655.

Atalla RH, Agarwal UP. 1985. Raman microprobe evidence for lignin orientation in the cell walls of native woody tissue. Science 227(4687):636–638.

Baskin TI, Beemster GTS, Judy-March JE, Marga F. 2004. Disorganization of cortical microtubules stimulates tangential expansion and reduces the uniformity of cellulose microfibril alignment among cells in the root of *arabidopsis*. Plant Physiol 135(4):2279–2290.

Cavalier DM, Lerouxel O, Neumetzler L, Yamauchi K, Reinecke A, Freshour G, Zabotina OA, Hahn MG, Burgert I, Pauly M, Raikhel NV, Keegstra K. 2008. Disrupting two *Arabidopsis thaliana* xylosyltransferase genes results in plants deficient in xyloglucan, a major primary cell wall component. Plant Cell 20(6):1519–1537.

Czaja AD, Kudryavtsev AB, Schopf JW. 2006. New method for the microscopic, nondestructive acquisition of ultraviolet resonance raman spectra from plant cell walls. Appl Spectrosc 60(4):352–355.

Dadi AP, Varanasi S, Schall CA. 2006. Enhancement of cellulose saccharification kinetics using an ionic liquid pretreatment step. Biotechnol Bioeng 95(5):904–910.

Davison B, Drescher S, Tuskan G, Davis M, Nghiem N. 2006. Variation of S/G ratio and lignin content in a populus family influences the release of xylose by dilute acid hydrolysis. Appl Biochem Biotechnol 130(1):427–435.

De Micco V, Aronne G. 2007. Combined histochemistry and autofluorescence for identifying lignin distribution in cell walls. Biotech Histochem 82(4):209–216.

D'Haeze W, Gao M, De Rycke R, Van Montagu M, Engler G, Holsters M. 2007. Roles for azorhizobial nod factors and surface polysaccharides in intercellular invasion and nodule penetration, respectively. Mol Plant Microbe Interact 11(10):999–1008.

Dokken KM, Davis LC, Marinkovic NS. 2005. Use of infrared microspectroscopy in plant growth and development. Appl Spectrosc Rev 40(4):301–326.

Evans CL, Xie XS. 2008. Coherent anti-stokes raman scattering microscopy: Chemical imaging for biology and medicine. Annu Rev Anal Chem 1(1):883–909.

Evert RF. 2007. Esau's plant anatomy: Meristems, cells, and tissues of the plant body: Their structure, function, and development. Hoboken, NJ: John Wiley & Sons, Inc.

Fagard M, Höfte H, Vernhettes S. 2000. Cell wall mutants. Plant Physiol Biochem 38(1–2):15–25.

Fenske JJ, Griffin DA, Penner MH. 1998. Comparison of aromatic monomers in lignocellulosic biomass prehydrolysates. J Ind Microbiol Biotechnol 20(6):364.

Freshour G, Bonin CP, Reiter W-D, Albersheim P, Darvill AG, Hahn MG. 2003. Distribution of fucose-containing xyloglucans in cell walls of the mur1 mutant of *arabidopsis*. Plant Physiol 131(4):1602–1612.

Fromm J, Rockel B, Lautner S, Windeisen E, Wanner G. 2003. Lignin distribution in wood cell walls determined by tem and backscattered sem techniques. J Struct Biol 143(1):77–84.

Galletti GC, Bocchini P, Smacchia AM III, JBR. 1996. Monitoring phenolic composition of maturing maize stover by high performance liquid chromatography and pyrolysis/gas chromatography/mass spectrometry. J Sci Food Agric 71(1):1–9.

Gallezot P. 2008. Catalytic conversion of biomass: Challenges and issues. ChemSusChem 1(8–9):734–737.

Gierlinger N, Schwanninger M. 2006. Chemical imaging of poplar wood cell walls by confocal raman microscopy. Plant Physiol 140(4):1246–1254.

Gierlinger N, Goswami L, Schmidt M, Burgert I, Coutand C, Rogge T, Schwanninger M. 2008a. In situ FT-IR microscopic study on enzymatic treatment of poplar wood cross-sections. Biomacromolecules 9(8): 2194–2201.

Gierlinger N, Sapei L, Paris O. 2008b. Insights into the chemical composition of equisetum hyemale by high resolution raman imaging. Planta 227(5):969–980.

Gomez LD, Steele-King CG, McQueen-Mason SJ. 2008. Sustainable liquid biofuels from biomass: The writing's on the walls. New Phytol 178(3): 473–485.

Grünwald C, Ruel K, Kim YS, Schmitt U. 2002. On the cytochemistry of cell wall formation in poplar trees. Plant Biol 4(1):13–21.

Harvey DJ. 2008. Analysis of carbohydrates and glycoconjugates by matrix-assisted laser desorption/ionization mass spectrometry: An update covering the period 2001–2002. Mass Spectrom Rev 27(2):125–201.

Hibberd JM, Quick WP. 2002. Characteristics of C_4 photosynthesis in stems and petioles of C_3 flowering plants. Nature 415(6870):451.

Himmel ME, Ding S-Y, Johnson DK, Adney WS, Nimlos MR, Brady JW, Foust TD. 2007. Biomass recalcitrance: Engineering plants and enzymes for biofuels production. Science 315(5813):804–807.

Jones L, Ennos AR, Turner SR. 2001. Cloning and characterization of *irregular xylem4* (*irx4*): A severely lignin-deficient mutant of *arabidopsis*. Plant J 26(2):205–216.

Kim H, Ralph J, Akiyama T. 2008. Solution-state 2d nmr of ball-milled plant cell wall gels in dmso-d6. Bioenergy Res 1(1):56–66.

Knox JP, Linstead PJ, King J, Cooper C, Roberts K. 1990. Pectin esterification is spatially regulated both within cell walls and between developing tissues of root apices. Planta 181(4):512–521.

Li C, Knierim B, Manisseri C, Arora R, Scheller HV, Auer M, Vogel KP, Simmons BA, Singh S. 2010. Comparison of dilute acid and ionic liquid pretreatment of switchgrass: Biomass recalcitrance, delignification and enzymatic saccharification. Bioresource Technol 101(13):4900–4906.

Niklas K, Paolillo D. 1997. The role of the epidermis as a stiffening agent in tulipa (liliaceae) stems. Am J Bot 84(6):735–744.

Percival Zhang YH, Himmel ME, Mielenz JR. 2006. Outlook for cellulase improvement: Screening and selection strategies. Biotechnol Adv 24(5): 452–481.

Persson S, Caffall KH, Freshour G, Hilley MT, Bauer S, Poindexter P, Hahn MG, Mohnen D, Somerville C. 2007a. The *arabidopsis* irregular xylem8 mutant is deficient in glucuronoxylan and homogalacturonan, which are essential for secondary cell wall integrity. Plant Cell 19(1): 237–255.

Persson S, Paredez A, Carroll A, Palsdottir H, Doblin M, Poindexter P, Khitrov N, Auer M, Somerville CR. 2007b. Genetic evidence for three unique components in primary cell-wall cellulose synthase complexes in *arabidopsis*. Proc Natl Acad Sci USA 104(39):15566–15571.

Pinto PC, Evtuguin DV, Neto CP. 2005. Effect of structural features of wood biopolymers on hardwood pulping and bleaching performance. Ind Eng Chem Res 44(26):9777–9784.

Saariaho A-M, Jääskeläinen A-S, Nuopponen M, Vuorinen T. 2003. Ultra violet resonance raman spectroscopy in lignin analysis: Determination of characteristic vibrations of *p*-hydroxyphenyl, guaiacyl, and syringyl lignin structures. Appl Spectrosc 57(1):58–66.

Schmidt M, Schwartzberg AM, Perera PN, Weber-Bargioni A, Carroll A, Sarkar P, Bosneaga E, Urban JJ, Song J, Balakshin MY, Capanema EA, Auer M, Adams PD, Chiang VL, Schuck PJ. 2009. Label-free in situ imaging of lignification in the cell wall of low lignin transgenic *Populus trichocarpa*. Planta 230(3): 589–597.

Simmons B, Loque D, Blanch H. 2008. Next-generation biomass feedstocks for biofuel production. Genome Biol 9(12):242.

Singh S, Simmons BA, Vogel KP. 2009. Visualization of biomass solubilization and cellulose regeneration during ionic liquid pretreatment of switchgrass. Biotechnol Bioeng 104(1):68–675.

Smith E, Dent G. 2005. Modern raman spectroscopy: A practical approach. Chichester, England: John Wiley & Sons Ltd.

Somerville C, Bauer S, Brininstool G, Facette M, Hamann T, Milne J, Osborne E, Paredez A, Persson S, Raab T, Vorwerk S, Youngs H. 2004. Toward a systems approach to understanding plant cell walls. Science 306(5705):2206–2211.

Spadiut O, Pisanelli I, Maischberger T, Peterbauer C, Gorton L, Chaiyen P, Haltrich D. 2009. Engineering of pyranose 2-oxidase: Improvement for biofuel cell and food applications through semi-rational protein design. J Biotechnol 139(3):250–257.

Teymouri F, Laureano-Perez L, Alizadeh H, Dale BE. 2005. Optimization of the ammonia fiber explosion (afex) treatment parameters for enzymatic hydrolysis of corn stover. Bioresource Technol 96(18):2014–2018.

Tilman D, Hill J, Lehman C. 2006. Carbon-negative biofuels from low-input high-diversity grassland biomass. Science 314(5805):1598–1600.

Tirumalai V, Agarwal U, Obst J. 1996. Heterogeneity of lignin concentration in cell corner middle lamella of white birch and black spruce. Wood Sci Technol 30(2):99–104.

Turner SR, Somerville CR. 1997. Collapsed xylem phenotype of *arabidopsis* identifies mutants deficient in cellulose deposition in the secondary cell wall. Plant Cell 9(5):689–701.

Vanholme R, Morreel K, Ralph J, Boerjan W. 2008. Lignin engineering. Curr Opin Plant Biol 11(3):278–285.

Weng J-K, Li X, Bonawitz ND, Chapple C. 2008. Emerging strategies of lignin engineering and degradation for cellulosic biofuel production. Curr Opin Biotechnol 19(2):166–172.

Williams M, Freshour G, Darvill AG, Albersheim P, Hahn MG. 1996. An antibody fab selected from a recombinant phage display library detects deesterified pectic polysaccharide rhamnogalacturonan II in plant cells. Plant Cell 8(4):673–685.

Wyman CE, Dale BE, Elander RT, Holtzapple M, Ladisch MR, Lee YY. 2005. Coordinated development of leading biomass pretreatment technologies. Bioresour Technol 96(18):1959–1966 .